A delayed mass-action model for the transcriptional control of Hmp, an NO detoxifying enzyme, by the iron-sulfur protein FNR

Marc R. Roussel

1 Introduction

Protein expression in living organisms involves, at minimum, two steps: transcription of the corresponding gene to a messenger RNA (mRNA), and translation of that mRNA to protein. Transcription and translation are among the slower processes in cells [1]. For a typical bacterial gene of 900 nt (nucleotides) [2], transcription at a rate of $24\,\mathrm{nt\,s^{-1}}$ [3] means that the mRNA is synthesized in 38 s. A 900 nt transcript encodes a 300 aa (amino acid) protein. Under optimal conditions, *Escherichia coli* ribosomes translate an mRNA at a rate of roughly $17\,\mathrm{aa\,s^{-1}}$ [4], so translation of a 300 aa protein transcript would take 18 s.

It is possible to model a gene expression network by including detailed models of transcription and translation, i.e. explicitly modeling every nucleotide addition to an mRNA, and every amino acid addition to a protein [5, 6, 7]. In most cases however, this is an undesirable level of detail, avoided by replacing the repetitive steps of transcription and translation by delays, which were perhaps first used in gene expression models in the 1970s [8, 9, 10].

As part of their immune response, mammals generate nitric oxide (NO), which inhibits a number of bacterial enzymes [11] and causes DNA damage. In many bacteria, Hmp, an enzyme that converts nitric oxide into nitrate ions, is a key part of the defenses against NO [11, 12]. Hmp is synthesized under the control of an NO-responsive repressor protein known as FNR [13]. Understanding the control system that regulates the production of Hmp could therefore prove useful in devising strategies for weakening bacterial defenses against nitrosative stress, thus helping the immune system combat pathogenic bacteria.

Tolla, Savageau and coworkers developed a model for FNR's role as a regulator of the aerobic/anaerobic metabolic switch in *E. coli* [14, 15], but did not consider

Marc R. Roussel
Alberta RNA Research and Training Institute, Department of Chemistry and Biochemistry, University of Lethbridge, Lethbridge, Alberta, Canada, T1K 3M4, e-mail: roussel@uleth.ca

FNR's role in the nitrosative stress response. Robinson and Brynildsen have constructed a general model for NO metabolism in *E. coli* [12, 16] that includes detoxification by Hmp. However, they use an empirical equation for the dependence of the rate of synthesis of Hmp on [NO]. In Sect. 2, a detailed biochemical model for the control of the synthesis of Hmp is developed, based on the delayed mass-action framework [17]. Parameter estimates are obtained in Sect. 3. The steady-state solutions of this model are studied in Sect. 4. The paper concludes with some perspectives for future work.

2 A model for the controlled synthesis of Hmp

We consider a cell that is exposed to an external source of nitric oxide, leading to a net inflow of this dissolved gas into the cytoplasm at a constant rate:

$$\xrightarrow{k_{\text{in}}} \text{NO}. \tag{1}$$

Hmp catalyzes the conversion of NO to nitrate [12]:

$$2\,\text{NO} + 2\,\text{O}_2 + \text{NAD(P)H} \longrightarrow 2\,{\text{NO}_3}^- + \text{NAD(P)}^+ + \text{H}^+$$

For catalysis to occur, the substrates must bind in order, NAD(P)H first, then O_2, then NO [18]. We can assume that the enzyme is constantly saturated with NADH or NADPH, given that the Michaelis constant of Hmp for NADH, the concentration of NADH required for half-maximal saturation of the enzyme, is $4.8\,\mu$M [18], and that the concentration of NADH in an *E. coli* cell is at least $83\,\mu$M [19]. The relevant reactions are therefore

$$\text{Hmp} + \text{O}_2 \underset{k_{-1}}{\overset{k_1}{\rightleftharpoons}} \text{Hmp}\cdot\text{O}_2, \tag{2a}$$

$$\text{Hmp}\cdot\text{O}_2 + \text{NO} \underset{k_{-2}}{\overset{k_2}{\rightleftharpoons}} \text{Hmp}\cdot\text{O}_2\cdot\text{NO} \xrightarrow{k_{-3}} \text{Hmp} + {\text{NO}_3}^-, \tag{2b}$$

$$\text{Hmp} + \text{NO} \underset{k_{-4}}{\overset{k_4}{\rightleftharpoons}} \text{Hmp}\cdot\text{NO}. \tag{2c}$$

(2c) is a substrate inhibition reaction, forming the catalytically inactive species $\text{Hmp}\cdot\text{NO}$. Each of these reactions is assumed to obey the law of mass-action, which states that the rate of an elementary reaction is proportional to the product of the reactant concentrations. The products are taken to appear instantaneously. The proportionality constant is known as a rate constant, and is written over (under) the arrow corresponding to the forward (reverse) reaction. For example, the rate of the forward reaction in (2a) is $k_1[\text{Hmp}][\text{O}_2]$.

Because of the recycling of RNA polymerase (RNAP) following the completion of transcription, the pool of free RNAP is roughly constant. Accordingly, we can subsume the dependence of the transcription initiation rate on [RNAP] into the cor-

responding rate constant. The transcription process can then be modeled as follows, using the delayed mass-action notation [17]:

$$\mathrm{Pro}^{hmp}(t) \xrightarrow{k_{tc}} \mathrm{Pro}^{hmp}(t+\tau_1) + \mathrm{RBS}^{hmp}(t+\tau_2), \tag{3}$$

where RBS^{hmp} represents the ribosome binding site of the mRNA. The interpretation of this equation is that, if there is a transcription initiation event at time t, the RNAP clears the promoter τ_1 time units later, and the ribosome binding site becomes available τ_2 time units later. The initiation event itself proceeds at a rate governed by the law of mass-action, in this case at a rate $k_{tc}[\mathrm{Pro}^{hmp}]$.

Translation of the mRNA can be similarly modeled, assuming a constant pool of ribosomes:

$$\mathrm{RBS}^{hmp}(t) \xrightarrow{k_{tl}} \mathrm{RBS}^{hmp}(t+\tau_3) + \mathrm{Hmp}(t+\tau_4). \tag{4}$$

τ_3 is the time required for the ribosome to clear the RBS, and τ_4 is the time required to translate the mRNA.

We must also consider the decay of the mRNA, which typically starts at the ribosome binding site, allowing translation events already initiated to run off [3, 20]. This explains the focus on the RBS in reactions (3) and (4).

$$\mathrm{RBS}^{hmp} \xrightarrow{k_5} \emptyset, \tag{5}$$

where $\emptyset$ represents decay products. Hmp also decays. We assume for simplicity that all of the enzyme-substrate complexes decay with similar kinetics:

$$\mathrm{Hmp} \xrightarrow{k_6} \emptyset, \tag{6a}$$

$$\mathrm{Hmp}\cdot\mathrm{O_2} \xrightarrow{k_6} \mathrm{O_2} + \emptyset, \tag{6b}$$

$$\mathrm{Hmp}\cdot\mathrm{O_2}\cdot\mathrm{NO} \xrightarrow{k_6} \mathrm{O_2} + \mathrm{NO} + \emptyset, \tag{6c}$$

$$\mathrm{Hmp}\cdot\mathrm{NO} \xrightarrow{k_6} \mathrm{NO} + \emptyset. \tag{6d}$$

Hmp transcription is repressed by FNR binding to the *hmp* promoter [21]. The active form of FNR (the holoprotein) is a dimer, with each monomer containing a [4 Fe – 4 S] cluster [22]. Reactions of the iron-sulfur cluster with NO cause the dimer to dissociate into its constituent monomers [21] and the affinity of FNR for the *hmp* promoter to decrease [23], allowing transcription to proceed. We focus here on the FNR monomer, for a number of reasons: First of all, the reactions at the two iron-sulfur clusters appear to be independent and to proceed with identical kinetics [21]. More importantly, dimerization of FNR or dissociation of these dimers is, under metabolic conditions, rapid and nearly quantitative [24].

Each iron-sulfur cluster reacts with NO in a 1:8 stoichiometry. This sequence of reactions is not fully understood at this time, so what follows, while based on the observations and interpretations of Crack and coworkers [21], will necessarily be somewhat speculative. Of the nine possible nitrosylation states, corresponding

to the addition of 0 to 8 NO molecules, only five, labeled A to E ($\mathrm{FNR_A} \equiv \mathrm{FNR}$, $\mathrm{FNR_B}$, …, $\mathrm{FNR_E}$), are kinetically distinguishable, and each of these is formed by a process which is kinetically of the first order in [NO]. The other four states are presumably transient species rapidly converted to kinetically more stable forms by further reactions with NO. The following is a plausible reaction sequence, based on the kinetic and spectroscopic analysis of Crack and coworkers:

$$\mathrm{FNR} + \mathrm{NO} \longrightarrow \mathrm{FNR_B}, \qquad v_{AB} = k_{AB}[\mathrm{FNR}][\mathrm{NO}]; \tag{7a}$$

$$\mathrm{FNR_B} + \mathrm{NO} \longrightarrow \mathrm{FNR_C}, \qquad v_{BC} = k_{BC}[\mathrm{FNR_B}][\mathrm{NO}]; \tag{7b}$$

$$\mathrm{FNR_C} + 2\,\mathrm{NO} \longrightarrow \mathrm{FNR_D}, \qquad v_{CD} = k_{CD}[\mathrm{FNR_C}][\mathrm{NO}]; \tag{7c}$$

$$\mathrm{FNR_D} + 4\,\mathrm{NO} \longrightarrow \mathrm{FNR_E}, \qquad v_{DE} = k_{DE}[\mathrm{FNR_D}][\mathrm{NO}]. \tag{7d}$$

Spectroscopic evidence indicates that $\mathrm{FNR_D}$ is the net product of the addition of four NO molecules [21], which required the allocation of an "extra" NO to one of reactions (7a) to (7c), arbitrarily added to (7c). Further assume that $\mathrm{FNR_E}$ is monomeric, unlike FNR A to D.

Not only does nitrosylated, monomerized FNR have a lower affinity for its DNA binding site than the holoprotein, it also has a lower specificity, i.e. it will bind to DNA sequences different from its natural binding site [23]. These two factors taken together along with the abundance of potential binding sites in the genome of a bacterial cell mean that very little of the monomerized form may bind to the promoter in the end. Therefore, assuming that $\mathrm{FNR_E}$ has negligible occupation of the promoter, repression of *hmp* by FNR is modeled by the following reactions:

$$\mathrm{Pro}^{hmp} + \mathrm{FNR} \underset{k_{-A}}{\overset{k_A}{\rightleftharpoons}} \mathrm{Pro}^{hmp} \cdot \mathrm{FNR}, \tag{8a}$$

$$\mathrm{Pro}^{hmp} + \mathrm{FNR_B} \underset{k_{-B}}{\overset{k_B}{\rightleftharpoons}} \mathrm{Pro}^{hmp} \cdot \mathrm{FNR_B}, \tag{8b}$$

$$\mathrm{Pro}^{hmp} + \mathrm{FNR_C} \underset{k_{-C}}{\overset{k_C}{\rightleftharpoons}} \mathrm{Pro}^{hmp} \cdot \mathrm{FNR_C}, \tag{8c}$$

$$\mathrm{Pro}^{hmp} + \mathrm{FNR_D} \underset{k_{-D}}{\overset{k_D}{\rightleftharpoons}} \mathrm{Pro}^{hmp} \cdot \mathrm{FNR_D}. \tag{8d}$$

It is not known whether NO can react with FNR bound to the promoter. However, oxygen does react with the FNR-promoter complex [25]. It is therefore likely that NO does too:

$$\mathrm{Pro}^{hmp} \cdot \mathrm{FNR} + \mathrm{NO} \longrightarrow \mathrm{Pro}^{hmp} \cdot \mathrm{FNR_B}, \qquad v_{AB}^{\mathrm{Pro}} = \alpha k_{AB}[\mathrm{Pro}^{hmp} \cdot \mathrm{FNR}][\mathrm{NO}]; \tag{9a}$$

$$\mathrm{Pro}^{hmp} \cdot \mathrm{FNR_B} + \mathrm{NO} \longrightarrow \mathrm{Pro}^{hmp} \cdot \mathrm{FNR_C}, \qquad v_{BC}^{\mathrm{Pro}} = \alpha k_{BC}[\mathrm{Pro}^{hmp} \cdot \mathrm{FNR_B}][\mathrm{NO}]; \tag{9b}$$

$$\mathrm{Pro}^{hmp} \cdot \mathrm{FNR_C} + 2\,\mathrm{NO} \longrightarrow \mathrm{Pro}^{hmp} \cdot \mathrm{FNR_D}, \qquad v_{CD}^{\mathrm{Pro}} = \alpha k_{CD}[\mathrm{Pro}^{hmp} \cdot \mathrm{FNR_C}][\mathrm{NO}]; \tag{9c}$$

$$\mathrm{Pro}^{hmp}\cdot\mathrm{FNR_D} + 4\,\mathrm{NO} \longrightarrow \mathrm{Pro}^{hmp} + \mathrm{FNR_E}, \quad v_{DE}^{\mathrm{Pro}} = \alpha k_{DE}[\mathrm{Pro}^{hmp}\cdot\mathrm{FNR_D}][\mathrm{NO}]. \tag{9d}$$

Note the dissociation of the monomerized $\mathrm{FNR_E}$ from the promoter in the last step. Lacking detailed information, the rate constants in reactions (9) are assumed to be uniformly scaled by a factor of α relative to those in reactions (7).

Dibden and Green showed that FNR recycling is more important than *de novo* protein synthesis [26] to the dynamics of this system, so a constant pool of FNR should be a good approximation. Let us suppose that the FNR recycling pathway operates on $\mathrm{FNR_E}$ in a reaction with effective first-order kinetics:

$$\mathrm{FNR_E} \xrightarrow{k_r} \mathrm{FNR}. \tag{10}$$

The Hmp-FNR model thus consists of reactions (1) to (10). The assumption of a constant pool of FNR leads to the following conservation law:

$$\begin{aligned}[\mathrm{FNR}]_{\mathrm{total}} &= [\mathrm{FNR}] + [\mathrm{FNR_B}] + [\mathrm{FNR_C}] + [\mathrm{FNR_D}] + [\mathrm{FNR_E}] \\ &+ [\mathrm{Pro}^{hmp}\cdot\mathrm{FNR}] + [\mathrm{Pro}^{hmp}\cdot\mathrm{FNR_B}] + [\mathrm{Pro}^{hmp}\cdot\mathrm{FNR_C}] + [\mathrm{Pro}^{hmp}\cdot\mathrm{FNR_D}].\end{aligned} \tag{11}$$

Assuming that the oxygen concentration is constant, the delayed mass-action framework [17] gives the following set of delay-differential equations (DDEs), using the notation $[\mathrm{A}]_{-\tau} \equiv [\mathrm{A}](t-\tau)$.

$$\begin{aligned}\frac{d[\mathrm{NO}]}{dt} &= k_{\mathrm{in}} - k_2[\mathrm{Hmp}\cdot\mathrm{O_2}][\mathrm{NO}] + k_{-2}[\mathrm{Hmp}\cdot\mathrm{O_2}\cdot\mathrm{NO}] - k_4[\mathrm{Hmp}][\mathrm{NO}] \\ &\quad + k_{-4}[\mathrm{Hmp}\cdot\mathrm{NO}] + k_6([\mathrm{Hmp}\cdot\mathrm{O_2}\cdot\mathrm{NO}] + [\mathrm{Hmp}\cdot\mathrm{NO}]) \\ &\quad - v_{AB} - v_{BC} - 2v_{CD} - 4v_{DE} - v_{AB}^{\mathrm{Pro}} - v_{BC}^{\mathrm{Pro}} - 2v_{CD}^{\mathrm{Pro}} - 4v_{DE}^{\mathrm{Pro}},\end{aligned} \tag{12a}$$

$$\begin{aligned}\frac{d[\mathrm{Hmp}]}{dt} &= -k_1[\mathrm{Hmp}][\mathrm{O_2}] + k_{-1}[\mathrm{Hmp}\cdot\mathrm{O_2}] + k_{-3}[\mathrm{Hmp}\cdot\mathrm{O_2}\cdot\mathrm{NO}] \\ &\quad - k_4[\mathrm{Hmp}][\mathrm{NO}] + k_{-4}[\mathrm{Hmp}\cdot\mathrm{NO}] + k_{tl}[\mathrm{RBS}^{hmp}]_{-\tau_4} - k_6[\mathrm{Hmp}],\end{aligned} \tag{12b}$$

$$\begin{aligned}\frac{d[\mathrm{Hmp}\cdot\mathrm{O_2}]}{dt} &= k_1[\mathrm{Hmp}][\mathrm{O_2}] - (k_{-1}+k_6)[\mathrm{Hmp}\cdot\mathrm{O_2}] \\ &\quad - k_2[\mathrm{Hmp}\cdot\mathrm{O_2}][\mathrm{NO}] + k_{-2}[\mathrm{Hmp}\cdot\mathrm{O_2}\cdot\mathrm{NO}],\end{aligned} \tag{12c}$$

$$\frac{d[\mathrm{Hmp}\cdot\mathrm{O_2}\cdot\mathrm{NO}]}{dt} = k_2[\mathrm{Hmp}\cdot\mathrm{O_2}][\mathrm{NO}] - (k_{-2}+k_{-3}+k_6)[\mathrm{Hmp}\cdot\mathrm{O_2}\cdot\mathrm{NO}], \tag{12d}$$

$$\frac{d[\mathrm{Hmp}\cdot\mathrm{NO}]}{dt} = k_4[\mathrm{Hmp}][\mathrm{NO}] - (k_{-4}+k_6)[\mathrm{Hmp}\cdot\mathrm{NO}], \tag{12e}$$

$$\begin{aligned}\frac{d[\mathrm{Pro}^{hmp}]}{dt} &= -k_{tc}[\mathrm{Pro}^{hmp}] + k_{tc}[\mathrm{Pro}^{hmp}]_{-\tau_1} - k_A[\mathrm{Pro}^{hmp}][\mathrm{FNR}] \\ &\quad + k_{-A}[\mathrm{Pro}^{hmp}\cdot\mathrm{FNR}] - k_B[\mathrm{Pro}^{hmp}][\mathrm{FNR_B}] + k_{-B}[\mathrm{Pro}^{hmp}\cdot\mathrm{FNR_B}] \\ &\quad - k_C[\mathrm{Pro}^{hmp}][\mathrm{FNR_C}] + k_{-C}[\mathrm{Pro}^{hmp}\cdot\mathrm{FNR_C}] - k_D[\mathrm{Pro}^{hmp}][\mathrm{FNR_D}] \\ &\quad + k_{-D}[\mathrm{Pro}^{hmp}\cdot\mathrm{FNR_D}] + v_{DE}^{\mathrm{Pro}},\end{aligned} \tag{12f}$$

$$\begin{aligned}\frac{d[\mathrm{RBS}^{hmp}]}{dt} &= k_{tc}[\mathrm{Pro}^{hmp}]_{-\tau_2} - k_{tl}[\mathrm{RBS}^{hmp}] + k_{tl}[\mathrm{RBS}^{hmp}]_{-\tau_3} \\ &\quad - k_5[\mathrm{RBS}^{hmp}],\end{aligned} \tag{12g}$$

$$\frac{d[\mathrm{FNR}]}{dt} = -v_{AB} - k_A[\mathrm{Pro}^{hmp}][\mathrm{FNR}] + k_{-A}[\mathrm{Pro}^{hmp}\cdot\mathrm{FNR}] + k_r[\mathrm{FNR_E}], \tag{12h}$$

$$\frac{d[\mathrm{FNR_B}]}{dt} = v_{AB} - v_{BC} - k_B[\mathrm{Pro}^{hmp}][\mathrm{FNR_B}] + k_{-B}[\mathrm{Pro}^{hmp}\cdot\mathrm{FNR_B}], \tag{12i}$$

$$\frac{d[\mathrm{FNR_C}]}{dt} = v_{BC} - v_{CD} - k_C[\mathrm{Pro}^{hmp}][\mathrm{FNR_C}] + k_{-C}[\mathrm{Pro}^{hmp}\cdot\mathrm{FNR_C}], \tag{12j}$$

$$\frac{d[\mathrm{FNR_D}]}{dt} = v_{CD} - v_{DE} - k_D[\mathrm{Pro}^{hmp}][\mathrm{FNR_D}] + k_{-D}[\mathrm{Pro}^{hmp}\cdot\mathrm{FNR_D}], \tag{12k}$$

$$\frac{d[\mathrm{FNR_E}]}{dt} = v_{DE} + v_{DE}^{\mathrm{Pro}} - k_r[\mathrm{FNR_E}], \tag{12l}$$

$$\frac{d[\mathrm{Pro}^{hmp}\cdot\mathrm{FNR}]}{dt} = k_A[\mathrm{Pro}^{hmp}][\mathrm{FNR}] - k_{-A}[\mathrm{Pro}^{hmp}\cdot\mathrm{FNR}] - v_{AB}^{\mathrm{Pro}}, \tag{12m}$$

$$\frac{d[\mathrm{Pro}^{hmp}\cdot\mathrm{FNR_B}]}{dt} = k_B[\mathrm{Pro}^{hmp}][\mathrm{FNR_B}] - k_{-B}[\mathrm{Pro}^{hmp}\cdot\mathrm{FNR_B}] + v_{AB}^{\mathrm{Pro}} - v_{BC}^{\mathrm{Pro}}, \tag{12n}$$

$$\frac{d[\mathrm{Pro}^{hmp}\cdot\mathrm{FNR_C}]}{dt} = k_C[\mathrm{Pro}^{hmp}][\mathrm{FNR_C}] - k_{-C}[\mathrm{Pro}^{hmp}\cdot\mathrm{FNR_C}] + v_{BC}^{\mathrm{Pro}} - v_{CD}^{\mathrm{Pro}}. \tag{12o}$$

In these equations, all terms are evaluated instantaneously unless otherwise noted. Production delays in reactions (3) and (4) give rise to the delayed terms in Eqs. (12b), (12f) and (12g).

Chemical rate equations, including delayed mass-action systems [17], are conservation equations describing the transformation of matter from one form to another. Delayed reactions can be understood using a pipe metaphor: the delayed terms represent matter that has entered a reaction channel and that will emerge from this channel at some later time. The material "in the pipe" must be accounted for in mass balances. The promoter in this model is neither created nor destroyed, although it is occluded by the polymerase for a period of time τ_1 following initiation of transcription [Eq. (3)]. This gives rise to an integral conservation relationship, which can be verified by differentiation with respect to time:

$$\begin{aligned}[\mathrm{Pro}^{hmp}]_{\mathrm{total}} &= [\mathrm{Pro}^{hmp}] + [\mathrm{Pro}^{hmp}\cdot\mathrm{FNR}] + [\mathrm{Pro}^{hmp}\cdot\mathrm{FNR_B}] + [\mathrm{Pro}^{hmp}\cdot\mathrm{FNR_C}] \\ &\quad + [\mathrm{Pro}^{hmp}\cdot\mathrm{FNR_D}] + k_{tc}\int_{t-\tau_1}^{t} [\mathrm{Pro}^{hmp}](t')\,dt'.\end{aligned} \tag{13}$$

3 Parameter estimates

This study targets physiological conditions for *E. coli*, which would imply among other things a temperature of 37 °C. The parameters for reactions (2) were generally taken from the kinetic study of Gardner and coworkers [18]. When rate constants were unavailable at 37 °C, the rule of thumb that rate constants roughly double for every 10-degree rise in temperature [27], corresponding to an activation energy of about $50\,\mathrm{kJ\,mol^{-1}}$, was used to estimate the rate constant at 37 °C.

In the lower gastrointestinal (GI) tract, the oxygen tension is about 11 torr [28]. The concentration of oxygen there can be calculated from the Henry's law coefficient of oxygen in water at 37 °C of $1.409 \times 10^{-6}\,\mathrm{M\,torr^{-1}}$ [29].

τ_1 can be estimated to be roughly 1.9 s based on the requirement for the polymerase to move 30 to 60 nt in order to clear the promoter [30], and the typical rate of transcription elongation of $24\,\mathrm{nt\,s^{-1}}$ [3]. Since there are no data on initiation frequencies from the *hmp* promoter, data from the well-characterized *lac* promoter are used instead, where under optimal conditions, transcription initiates on average every 3.3 s [31]. Given that 1.9 s is spent clearing the promoter, this means that the average wait time for initiation at an empty promoter is 1.4 s, corresponding to a rate constant of $k_{tc} = 0.71\,\mathrm{s^{-1}}$. The transcriptional delay τ_2 was estimated from the gene length for Hmp (1191 nt [32]) and the elongation rate.

For translation, given an RBS clearance time of approximately 2 s [33] and a mean time between translation initiations, again for the *lac* transcript, of 3.2 s [31], we can calculate a translation initiation rate constant of $k_{tl} = 0.83\,\mathrm{s^{-1}}$. At a translation rate of $17\,\mathrm{aa\,s^{-1}}$ [4], the 396 aa Hmp protein would be translated in a time $\tau_4 = 23\,\mathrm{s}$. This estimate assumes that transcription and translation are spatially and temporally separated, in accord with recent evidence in *E. coli* [34].

Throughout this paper, we assume that an *E. coli* cell has a volume of 1.7 fL [35].

Cell growth has the effect of diluting the cellular contents. Under anaerobic conditions, *E. coli* grows at a median rate of $0.25\,\mathrm{h^{-1}}$ [36]. Adding this to the chemical decay constant calculated from the 66 min half-life of Hmp in *Salmonella* Typhimurium [37], we obtain an effective value of k_6 of $2.4 \times 10^{-4}\,\mathrm{s^{-1}}$.

The *in vivo* concentration of FNR can be calculated from the number of molecules of FNR present in an *E. coli* cell grown at 37 °C under anaerobic conditions, which is approximately 2600 [38].

For reactions (8), if we assume a typical bimolecular rate constant for all four steps of $10^7\,\mathrm{M^{-1}\,s^{-1}}$ (similar to the rate constant for binding of the structurally related protein CAP to the *lac* operator [39]), then we can calculate the dissociation rate constants given the dissociation equilibrium constants (K_d). For the holoprotein, $K_d = 1 \times 10^{-6}\,\mathrm{M}$ [23]. It is also known that adding NO loosens the complex. Assuming a moderate loosening (i.e. an increase in K_d) of $0.5 \times 10^{-6}\,\mathrm{M}$ per step keeps the K_d within the measured range for nitrosylated FNR [23].

All of the parameter estimates obtained are shown in Table 1. The only model parameters not estimated in this section are k_r and α, for which literature values are not available, and k_{in}, which is treated as a control parameter in this study.

Table 1 Model parameters. Values carrying the notation $[T]$ in the reference field were adjusted for temperature as described in the text. The notation [a] indicates an assumed value, while [c] indicates that the value was calculated as described in the text. The [s] notation indicates that data from *E. coli* were unavailable and that data from another bacterial species were therefore used. For k_{-A}, the first value given was calculated in Sect. 3, and the second is proposed in Sect. 4.

Parameter	Value	Reference	Parameter	Value	Reference
Hmp catalysis			*FNR dynamics*		
$[O_2]$	$16\,\mu$M	[c]	$[\text{FNR}]_{\text{total}}$	$2.5\,\mu$M	[c]
k_1	$8\times10^6\,\text{M}^{-1}\text{s}^{-1}$	[18]	k_{AB}	$6.1\times10^5\,\text{M}^{-1}\text{s}^{-1}$	[21][T]
k_{-1}	$1.4\,\text{s}^{-1}$	[18][T]	k_{BC}	$4.1\times10^4\,\text{M}^{-1}\text{s}^{-1}$	[21][T]
k_2	$2.5\times10^9\,\text{M}^{-1}\text{s}^{-1}$	[18]	k_{CD}	$1.0\times10^4\,\text{M}^{-1}\text{s}^{-1}$	[21][T]
k_{-2}	$6.2\times10^{-4}\,\text{s}^{-1}$	[18][T]	k_{DE}	$1.6\times10^3\,\text{M}^{-1}\text{s}^{-1}$	[21][T]
k_{-3}	$6.2\times10^2\,\text{s}^{-1}$	[18][T]	α	1	[a]
k_4	$8.0\times10^7\,\text{M}^{-1}\text{s}^{-1}$	[18][T]	k_A	$10^7\,\text{M}^{-1}\text{s}^{-1}$	[a]
k_{-4}	$6.2\times10^{-4}\,\text{s}^{-1}$	[18][T]	k_{-A}	$10\,\text{s}^{-1}\rightarrow0.11\,\text{s}^{-1}$	[c]
Hmp expression			k_B	$10^7\,\text{M}^{-1}\text{s}^{-1}$	[a]
k_{tc}	$0.71\,\text{s}^{-1}$	[c]	k_{-B}	$15\,\text{s}^{-1}$	[c]
τ_1	1.9 s	[c]	k_C	$10^7\,\text{M}^{-1}\text{s}^{-1}$	[a]
τ_2	50 s	[c]	k_{-C}	$20\,\text{s}^{-1}$	[c]
k_{tl}	$0.83\,\text{s}^{-1}$	[c]	k_D	$10^7\,\text{M}^{-1}\text{s}^{-1}$	[a]
τ_3	2 s	[33]	k_{-D}	$25\,\text{s}^{-1}$	[c]
τ_4	23 s	[c]	k_r	$0.1\,\text{s}^{-1}$	[a]
k_5	$0.014\,\text{s}^{-1}$	[40][s]			
k_6	$2.4\times10^{-4}\,\text{s}^{-1}$	[c]			

4 Steady-state analysis

In the steady state, Eq. (13) becomes

$$[\text{Pro}^{hmp}]_{\text{total}} = [\text{Pro}^{hmp}](1+k_{tc}\tau_1) + [\text{Pro}^{hmp}\cdot\text{FNR}] + [\text{Pro}^{hmp}\cdot\text{FNR}_\text{B}] + [\text{Pro}^{hmp}\cdot\text{FNR}_\text{C}] + [\text{Pro}^{hmp}\cdot\text{FNR}_\text{D}]. \quad (14)$$

The steady states satisfy Eqs. (11), (12a)–(12e), (12g)–(12o) and (14). Since, in a steady state, $x(t-\tau)=x(t)$, the values of the delays typically drop out of the steady-state analysis of models with delays. This is not necessarily the case in gene expression models, as we see here. The delay τ_1, while small, has an effect on the steady state via Eq. (14) because it accounts for the period during which access to the promoter is blocked by the polymerase. Note that $k_{tc}\tau_1 = 1.3 \sim 1$, so τ_1 is not negligible.

The steady-state equations were solved in Maple using the `fsolve()` function. Branches of steady states were followed by taking small steps along a branch and using the solution at the last step as an initial guess.

The NO-free ($k_{\text{in}}=0$) steady state using the parameters of Table 1, with $k_{-A} = 10\,\text{s}^{-1}$ as calculated in the previous section, and $[\text{Pro}^{hmp}]_{\text{total}} = 0.98\,\text{nM}$, corresponding to one promoter per cell, has $[\text{Pro}^{hmp}] = 0.20\,\text{nM}$ and $[\text{Pro}^{hmp}\cdot\text{FNR}] = 0.51\,\text{nM}$.

The remaining 0.27 nM of the promoter is "in the pipe", i.e. occluded by a polymerase. A single promoter cannot be divided in this manner. Rather, we should think about these "concentrations" as being related to probabilities over a large ensemble of cells. In particular, only 52% of the *hmp* promoters in an ensemble of cells are repressed at any given time. The rest are either waiting for a polymerase, or have a polymerase engaged in transcription initiation. As a result, the total Hmp concentration in this calculation is very high ($[\mathrm{Hmp}] + [\mathrm{Hmp}\cdot\mathrm{O_2}] = 35\,\mu\mathrm{M}$). In the absence of NO however, we expect a low level of Hmp. A lower level of Hmp expression could be obtained by lowering k_{tc}, a parameter estimated based on data from a different gene. However, the very low level of repression of the *hmp* promoter, which depends on an experimentally measured K_d [23], seems more anomalous than does the value of k_{tc}. Thus assume, arbitrarily, that the affinity of holo-FNR for the *hmp* promoter is sufficiently high for 99% repression. Given the large size assumed for k_A, k_{-A} is adjusted to a value of $0.11\,\mathrm{s}^{-1}$, a hundredfold lower than the estimate of Sect. 3. The rate constants associated with the binding of the nitrosylated forms of FNR to DNA have not been adjusted, on the assumption that there is a significant drop-off in affinity as FNR is progressively nitrosylated.

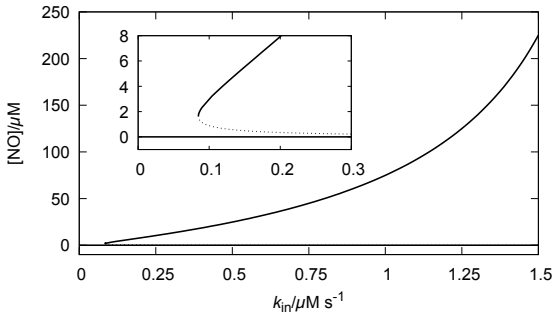

Fig. 1 Steady states of the model vs k_{in} obtained for the parameters of Table 1 with the lower value of k_{-A}. The initial conditions were chosen to correspond to one promoter per cell. The inset is a blowup of the small-k_{in} region. Solid curves: stable steady states; dotted curve: unstable steady state.

Figure 1 shows a bifurcation diagram obtained by numerically following branches of solutions in Maple as described above. As k_{in} increases from zero, a bifurcation to bistability occurs near $k_{\mathrm{in}} = 0.084\,783\,\mu\mathrm{M}s^{-1}$, with two branches of stable steady states (verified by numerical integration of the DDEs (12) supplemented by the conservation relation (11) using the "stiff" integrator in XPPAUT [41]) separated by a branch of unstable steady states. In the bistable region, the lower branch corresponds to the desired behavior as the sub-nanomolar concentrations obtained here correspond to less than one molecule of NO per cell. In this steady state, $\mathrm{Hmp}\cdot\mathrm{O_2}$ is the dominant form of the Hmp enzyme (Fig. 2). Accordingly, the cell's biochemical state is primed for NO detoxification, and NO does not accumulate. In the high-NO steady state, the unproductive complex $\mathrm{Hmp}\cdot\mathrm{NO}$ has become dominant (Fig. 2). Because k_4 is approximately ten times larger than k_1, once an enzyme has completed a cycle of catalysis, at high NO levels, it becomes more likely to add a molecule of NO than a molecule of $\mathrm{O_2}$. The small value of k_{-4} then results in very effective in-

hibition of Hmp's catalytic activity. The high-NO state is therefore self-reinforcing, leading to the observed bistability. Note that substrate inhibition has previously been shown to be a potential cause of bistability in biochemical systems [42, 43, 44].

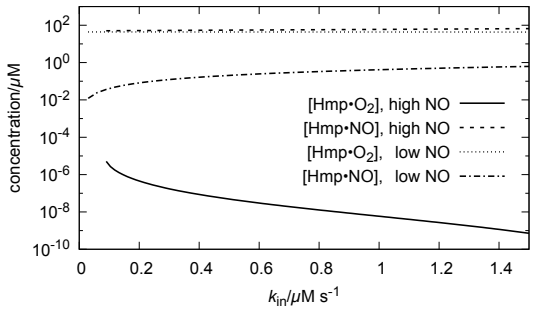

Fig. 2 Concentrations of key complexes of Hmp for the high- and low-NO steady states shown in Fig. 1.

It may be asked whether the *ad hoc* adjustment of k_{-A} had any effect on the results. A bifurcation diagram computed with the larger value of k_{-A} (not shown) is identical to the one shown in Fig. 1 to within the numerical resolution of the calculations. There are differences in some variables, particularly at lower values of k_{in}, but the NO concentration being the key variable from the point of view of the cell's health, we can conclude that the network's steady-state response is robust with respect to the value of k_{-A}. The model with a lower value of k_{-A} is much less wasteful, accumulating roughly half as much Hmp (all forms combined) at lower values of k_{in} (below about $0.1\,\mu\text{M}\,\text{s}^{-1}$; data not shown). Further calculations were carried out, again somewhat arbitrarily, with the lower value of k_{-A}.

The unknown parameters k_r and α were varied (results not shown). Neither of these parameters changes the qualitative dynamics. While there are clear quantitative effects associated with varying k_r, notably a steep increase in the high-NO steady state at lower values of k_r, the solutions are remarkably insensitive to α.

E. coli experiences varied oxygen concentrations during its life cycle, including its transit through the GI tract [28]. We would expect that higher O_2 concentrations would shift the balance towards the $\text{Hmp}\cdot\text{O}_2$ complex relative to the $\text{Hmp}\cdot\text{NO}$ complex, and thus increase the rate of NO removal, possibly abolishing bistability. The latter hypothesis is correct, as can be seen in Fig. 3. However, the oxygen concentrations at which bistability gives way to a monostable low-[NO] solution are unrealistically high. For comparison, consider that water in equilibrium with air at normal atmospheric pressure at 37 °C would hold $225\,\mu\text{M}$ of dissolved O_2. The saddle-node bifurcation at $[\text{O}_2] \approx 596\,\mu\text{M}$ is therefore of no physiological consequence.

Robinson and Brynildsen used the following empirical equation to model the net dependence of the translation rate of Hmp on [NO] [16]:

$$v_{\text{tl}}^{\text{RB2016}} = k_{\text{basal}} + (k_{\text{max}} - k_{\text{basal}})[\text{NO}]/\left(K_{\text{NO}} + [\text{NO}]\right). \tag{15}$$

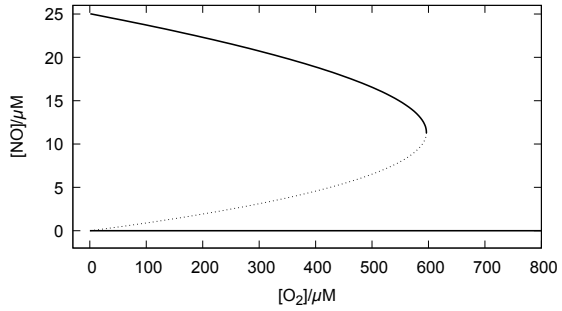

Fig. 3 Steady states as a function of $[O_2]$. All parameters are as in Fig. 1 with $k_{\text{in}} = 0.5\,\mu\text{M}$.

We can compute the steady-state translation rate in the Hmp-FNR model, $v_{\text{tl}} = k_{\text{tl}}[\text{RBS}^{hmp}]$, with [NO] as a parameter, by dropping Eq. (12a) and solving the remaining steady-state conditions, including the conservation equations (11) and (14). The solid curve in Fig. 4 is the rate of translation calculated from the Hmp-FNR model. Treating [NO] as a parameter eliminates the feedback that leads to bistability, and only one steady state is found for any given value of [NO]. Interestingly, this steady state is a high-[Hmp·NO] steady state. Coupling of the NO concentration to the catalytic degradation of NO by Hmp is thus critical to the creation of the low-[NO], low-[Hmp·NO] steady state that allows cells to survive nitrosative stress. The dashed curve in Fig. 4 is the best fit of Eq. (15) to the steady-state translation rate curve over the concentration range shown in the figure. The shape of the translation curve generated by the Hmp-FNR model is clearly quite different from the shape assumed by Robinson and Brynildsen. Whether this has any material effect on the results of their calculations is unknown.

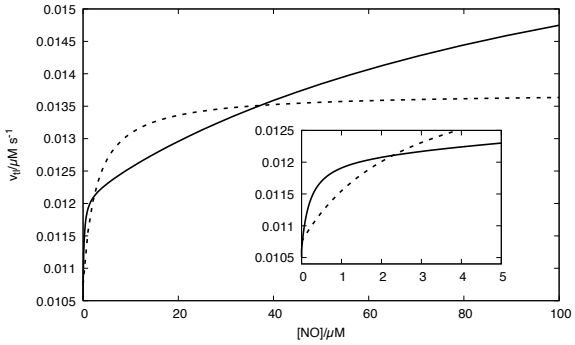

Fig. 4 Steady-state translation curve from the Hmp-FNR model (solid curve), treating [NO] as a parameter, for the parameters of Table 1 using the lower value of k_{-A}. The dashed curve is a fit of Eq. (15) to the translation rate from the Hmp-FNR model, yielding $k_{\text{basal}} = 0.01075\,\mu\text{M}\,\text{s}^{-1}$, $k_{\text{max}} = 0.01371\,\mu\text{M}\,\text{s}^{-1}$, and $K_{\text{NO}} = 2.7\,\mu\text{M}$. The inset magnifies the small-[NO] region.

5 Discussion and conclusions

The reactions in this model were, insofar as was possible, drawn from the literature. Still, the model contains some assumptions whose effects on the qualitative and quantitative behavior of the solutions are yet to be examined. Perhaps the most important modeling decision was the focus on nitrosylation states of monomers rather than explicitly considering dimers. A lumping analysis [45] to be presented elsewhere however suggests that this is a tenable approximation.

It is possible that the low-NO steady state is selected by additional regulatory or biochemical interactions. For instance, in *E. coli*, *hmp* transcription is regulated both by FNR and by NsrR [46]. NsrR is, like FNR, an iron-sulfur protein that represses *hmp* transcription while its iron-sulfur cluster is intact. The kinetics of nitrosylation of the iron-sulfur cluster in NsrR is analogous to that of FNR [47]. It would be interesting to model the joint control of *hmp* transcription by FNR and NsrR.

Fig. 1 suggests that, in the bistable range, the basin of attraction of the desired low-NO steady state is relatively small with respect to the NO concentration, neglecting the dependence of this basin on the initial function [48]. *In vivo*, the NO inflow rate (k_{in}) will not be a fixed parameter but will have a time course dictated by the dynamics of the immune system and by the kinetics of permeation of NO through the cell membrane. Accordingly, it would be interesting to study the basin of attraction of the low-NO steady state with respect to a family of parameterized temporal programs for $k_{\text{in}}(t)$. Is there a critical rate of increase of k_{in} beyond which the system jumps to the high-NO steady state? How long and how intense a pulse of NO can the system handle and still return to the low-NO steady state?

In principle, all of the delays can be manipulated experimentally by changing the gene's sequence. In particular, the promoter clearance delay τ_1 hides a number of mechanistic details, including repeated rounds of abortive initiation, during which the polymerase "scrunches" the DNA as it adds the first few nucleotides to the new mRNA, then either releases an abortive transcript and returns to its starting position, or escapes from the promoter [49]. The mean number of cycles of abortive initiation, and thus the mean promoter clearance time, depends on the sequence of the promoter and of the initially transcribed region [50]. Whether there are any qualitative changes in the behavior of the model over a plausible range of τ_1 values remains to be seen.

Gene expression raises a modeling complication not addressed here, namely that of the low copy numbers of various species. For instance, the number of active promoters is not a continuous variable as modeled here, but a discrete one that can only take on integer values, limited by the gene copy number. Similarly, free ribosome binding site (mRNA) concentrations generated by this model correspond to one to two dozen molecules per cell, again in a range where a continuous description is problematic. A differential equation model provides population-level average behavior, but it cannot describe the dynamics in a single cell. Accordingly, we need models that incorporate both delays and stochasticity due to finite populations. Methods for simulating systems with these two features have recently been developed [51, 52, 53, 54], and software implementing some of these algorithms is

available [55, 56]. In addition to finite population effects, the intrinsic unpredictability of certain processes, such as the random number of rounds of abortive initiation prior to promoter escape, are more easily incorporated into a stochastic model than into a differential equation model. Studying a stochastic counterpart of the DDE model described here is therefore an important next step for this project.

Acknowledgements I would like to thank Professor Nick Le Brun of the University of East Anglia for answering some of my questions about this system. This work was supported by the Natural Sciences and Engineering Research Council of Canada.

References

1. M. Shamir, Y. Bar-On, R. Phillips, R. Milo, Cell **164**, 1302 (2016). DOI 10.1016/j.cell.2016.02.058
2. L. Xu, H. Chen, X. Hu, R. Zhang, Z. Zhang, Z.W. Luo, Mol. Biol. Evol. **23**, 1107 (2006). DOI 10.1093/molbev/msk019
3. H. Chen, K. Shiroguchi, H. Ge, X.S. Xie, Mol. Syst. Biol. **11**, 781 (2015). DOI 10.15252/msb.20145794. Errata: Mol. Syst. Biol. **11**, 808 (2015). DOI 10.15252/msb.20159000
4. R. Young, H. Bremer, Biochem. J. **160**, 185 (1976). DOI 10.1042/bj1600185
5. M.R. Roussel, R. Zhu, Bull. Math. Biol. **68**, 1681 (2006). DOI 10.1007/s11538-005-9048-6
6. I. Potapov, J. Lloyd-Price, O. Yli-Harja, A.S. Ribeiro, Phys. Rev. E **84**, 031903 (2011). DOI 10.1103/PhysRevE.84.031903
7. I. Potapov, J. Mäkelä, O. Yli-Harja, A.S. Ribeiro, J. Theor. Biol. **315**, 17 (2012). DOI 10.1016/j.jtbi.2012.08.029
8. N. MacDonald, J. Theor. Biol. **67**, 549 (1977). DOI 10.1016/0022-5193(77)90056-X
9. R.D. Bliss, Analysis of the dynamic behavior of the tryptophan operon of *Escherichia coli*: The functional significance of feedback inhibition. Ph.D. thesis, University of California Riverside (1979)
10. U. an der Heiden, J. Math. Biol. **8**, 345 (1979). DOI 10.1007/BF00275831
11. R.K. Poole, Biochem. Soc. Trans. **33**, 176 (2005). DOI 10.1042/BST0330176
12. J.L. Robinson, M.P. Brynildsen, PLoS Comput. Biol. **9**, e1003049 (2013). DOI 10.1371/journal.pcbi.1003049
13. R.K. Poole, M.N. Hughes, Mol. Microbiol. **36**, 775 (2000). DOI 10.1046/j.1365-2958.2000.01889.x
14. D.A. Tolla, M.A. Savageau, J. Mol. Biol. **397**, 893 (2010). DOI 10.1016/j.jmb.2010.02.015
15. D.A. Tolla, P.J. Kiley, J.G. Lomnitz, M.A. Savageau, Mol. Biosyst. **11**, 1841 (2015). DOI 10.1039/c5mb00055f
16. J.L. Robinson, M.P. Brynildsen, Proc. Natl. Acad. Sci. U.S.A. **113**, E1757 (2016). DOI 10.1073/pnas.1521354113
17. M.R. Roussel, J. Phys. Chem. **100**, 8323 (1996). DOI 10.1021/jp9600672
18. A.M. Gardner, L.A. Martin, P.R. Gardner, Y. Dou, J.S. Olson, J. Biol. Chem. **275**, 12581 (2000). DOI 10.1074/jbc.275.17.12581
19. B.D. Bennett, E.H. Kimball, M. Gao, R. Osterhout, S.J. Van Dien, J.D. Rabinowitz, Nat. Chem. Biol. **5**, 593 (2009). DOI 10.1038/nchembio.186
20. D. Kennell, V. Talkad, J. Mol. Biol. **104**, 285 (1976). DOI 10.1016/0022-2836(76)90014-0
21. J.C. Crack, M.R. Stapleton, J. Green, A.J. Thomson, N.E. Le Brun, J. Biol. Chem. **288**, 11492 (2013). DOI 10.1074/jbc.M112.439901
22. P.J. Kiley, H. Beinert, FEMS Microbiol. Rev. **22**, 341 (1999). DOI 10.1111/j.1574-6976.1998.tb00375.x

23. H. Cruz-Ramos, J. Crack, G. Wu, M.N. Hughes, C. Scott, A.J. Thomson, J. Green, R.K. Poole, EMBO J. **21**, 3235 (2002). DOI 10.1093/emboj/cdf339
24. B.A. Lazazzera, H. Beinert, N. Khoroshilova, M.C. Kennedy, P.J. Kiley, J. Biol. Chem. **271**, 2762 (1996). DOI 10.1074/jbc.271.5.2762
25. J.C. Crack, M.R. Stapleton, J. Green, A.J. Thomson, N.E. Le Brun, Biochem. J. **463**, 83 (2014). DOI 10.1042/BJ20140169
26. D.P. Dibden, J. Green, Microbiology **151**, 4063 (2005). DOI 10.1099/mic.0.28253-0
27. L. Pauling, *General Chemistry* (Dover, New York, 1988)
28. G. He, R.A. Shankar, M. Chzhan, A. Samouilov, P. Kuppusamy, J.L. Zweier, Proc. Natl. Acad. Sci. U.S.A. **96**, 4586 (1999). DOI 10.1073/pnas.96.8.4586
29. T.R. Rettich, R. Battino, E. Wilhelm, J. Chem. Thermodynamics **32**, 1145 (2000). DOI 10.1006/jcht.1999.0581
30. M.T. Record, Jr., W.S. Reznikoff, M.L. Craig, K.L. McQuade, P.J. Schlax, in Escherichia coli *and* Salmonella*: Cellular and Molecular Biology*, vol. 2, ed. by F.C. Neidhardt, 2nd edn. (ASM Press, Washington, 1996), pp. 792–820
31. D. Kennell, H. Riezman, J. Mol. Biol. **114**, 1 (1977). DOI 10.1016/0022-2836(77)90279-0
32. S.G. Vasudevan, W.L.F. Armarego, D.C. Shaw, P.E. Lilley, N.E. Dixon, R.K. Poole, Mol. Gen. Genet. **226**, 49 (1991). DOI 10.1007/BF00273586
33. A.S. Ribeiro, Math. Biosci. **223**, 1 (2010). DOI 10.1016/j.mbs.2009.10.007
34. S. Bakshi, A. Siryaporn, M. Goulian, J.C. Weisshaar, Mol. Microbiol. **85**, 21 (2012). DOI 10.1111/j.1365-2958.2012.08081.x
35. N. Grossman, E.Z. Ron, C.L. Woldringh, J. Bacteriol. **152**, 35 (1982)
36. A. Hasona, Y. Kim, F.G. Healy, L.O. Ingram, K.T. Shanmugam, J. Bacteriol. **186**, 7593 (2004). DOI 10.1128/JB.186.22.7593-7600.2004
37. Z. Wang, Q.Q. Han, M.T. Zhou, X. Chen, L. Guo, J. Basic Microbiol. **56**, 801 (2016). DOI 10.1002/jobm.201500315
38. V.R. Sutton, E.L. Mettert, H. Beinert, P.J. Kiley, J. Bacteriol. **186**, 8018 (2004). DOI 10.1128/JB.186.23.8018-8025.2004
39. J.T. Gerstle, M.G. Fried, Electrophoresis **14**, 725 (1993). DOI 10.1002/elps.11501401115
40. Y. Hu, P.D. Butcher, J.A. Mangan, M.A. Rajandream, A.R.M. Coates, J. Bacteriol. **181**, 3486 (1999)
41. B. Ermentrout, *Simulating, Analyzing, and Animating Dynamical Systems* (SIAM, Philadelphia, 2002)
42. H. Degn, Nature **217**, 1047 (1968). DOI 10.1038/2171047b0
43. F.F. Seelig, B. Denzel, FEBS Lett. **24**, 283 (1972). DOI 10.1016/0014-5793(72)80373-9
44. B.D. Aguda, Biophys. Chem. **61**, 1 (1996). DOI 10.1016/0301-4622(96)00019-1
45. J. Wei, J.C.W. Kuo, Ind. Eng. Chem. Fundam. **8**, 114 (1969). DOI 10.1021/i160029a019
46. D.A. Rodionov, I.L. Dubchak, A.P. Arkin, E.J. Alm, M.S. Gelfrand, PLoS Comput. Biol. **1**, e55 (2005). DOI 10.1371/journal.pcbi.0010055
47. J.C. Crack, D.A. Svistunenko, J. Munnoch, A.J. Thomson, M.I. Hutchings, N.E. Le Brun, J. Biol. Chem. **291**, 8663 (2016). DOI 10.1074/jbc.M115.693192
48. S.R. Taylor, S.A. Campbell, Phys. Rev. E **75**, 046215 (2007). DOI 10.1103/PhysRevE.75.046215
49. A.N. Kapanidis, E. Margeat, S.O. Ho, E. Kortkhonjia, S. Weiss, R.H. Ebright, Science **314**, 1144 (2006). DOI 10.1126/science.1131399
50. J. Skancke, N. Bar, M. Kuiper, L.M. Hsu, Biochemistry **54**, 4267 (2015). DOI 10.1021/acs.biochem.5b00272
51. M.A. Gibson, J. Bruck, J. Phys. Chem. A **104**, 1876 (2000). DOI 10.1021/jp993732q
52. D. Bratsun, D. Volfson, L.S. Tsimring, J. Hasty, Proc. Natl. Acad. Sci. U.S.A. **102**, 14593 (2005). DOI 10.1073/pnas.0503858102
53. M. Barrio, K. Burrage, A. Leier, T. Tian, PLoS Comput. Biol. **2**, e117 (2006). DOI 10.1371/journal.pcbi.0020117
54. M.R. Roussel, R. Zhu, Phys. Biol. **3**, 274 (2006). DOI 10.1088/1478-3975/3/4/005
55. S. Ramsey, D. Orrell, H. Bolouri, J. Bioinform. Comput. Biol. **3**, 415 (2005). DOI 10.1142/S0219720005001132
56. J. Lloyd-Price, A. Gupta, A.S. Ribeiro, Bioinformatics **28**, 3004 (2012). DOI 10.1093/bioinformatics/bts556